*Anal. Chem.* **2007,** *79,* 4094−4100

# On-Chip Surface-Based Detection with Nanohole Arrays

**Angela De Leebeeck,† L. K. Swaroop Kumar,‡ Victoria de Lange,‡ David Sinton,*,† Reuven Gordon,*,‡ and Alexandre G. Brolo*,§**

*Department of Mechanical Engineering, Department of Electrical and Computer Engineering, and Department of Chemistry, University of Victoria, Victoria, BC, Canada*

**A microfluidic device with integrated surface plasmon resonance (SPR) chemical and biological sensors based on arrays of nanoholes in gold films is demonstrated. Widespread use of SPR for surface analysis in laboratories has not translated to microfluidic analytical chip platforms, in part due to challenges associated with scaling down the optics and the surface area required for common reflection mode operation. The resonant enhancement of light transmission through subwavelength apertures in a metallic film suggests the use of nanohole arrays as miniaturized SPR-based sensing elements. The device presented here takes advantage of the unique properties of nanohole arrays: surface-based sensitivity; transmission mode operation; a relatively small footprint; and repeatability. Proof-of-concept measurements performed on-chip indicated a response to small changes in refractive index at the array surfaces. A sensitivity of 333 nm per refractive index unit was demonstrated with the integrated device. The device was also applied to detect spatial microfluidic concentration gradients and to monitor a biochemical affinity process involving the biotin−streptavidin system. Results indicate the efficacy of nanohole arrays as surface plasmon-based sensing elements in a microfluidic platform, adding unique surface-sensitive diagnostic capabilities to the existing suite of microfluidic-based analytical tools.**

Surface plasmons (SPs) are surface-bound electromagnetic waves formed at the interface between a metal and a dielectric. Although SPs from a smooth metallic surface cannot be directly excited by light, the surface plasmon resonance (SPR) condition can be achieved by either prism or grating coupling.[1,2] Due to their interfacial nature, SPs are very sensitive to the near-surface dielectric constant (index of refraction) and are well-suited to the detection of surface binding events. This characteristic has been exploited in a wide variety of SPR-based sensors, particularly biosensors,[3,4] for which commercial devices are available.[5] The most common methodology involves the Kretschmann configuration,[1] where a prism is used for the light−SP coupling at the surface of a thin gold film (∼50 nm). The probe light undergoes total internal reflection on the inner surface of the prism. At the SPR angle, an evanescent light field travels through the gold thin film and excites SPs at the metal−dielectric interface, reducing the intensity of the reflected light. The SPR angle is sensitive to several factors,[6] including the wavelength of light, the thickness of the gold film, the physical and optical properties of the prism, and the index of refraction of the medium near the metallic interface (which is typically <200 nm[6]). The latter sensitivity, combined with signal averaging over a relatively large area,[7] is commonly exploited in these sensor applications. Device-level miniaturization of SPR-based sensing and integration with microfluidics has been limited,[7,8] in part due to the following: the utility of averaging over a large surface; the challenges associated with scaling down the prism and optical infrastructure needed for reflection mode operation; and difficulty in incorporating high numerical aperture optics to achieve high spatial resolution. Recently, SPR reflectance imaging was applied to monitor concentration during the replacement of water with ethanol in a straight microfluidic channel[7] and to visualize the mixing in a flow cell.[8] In those studies, the prism surface comprised one wall of the microchannel, and the concentration changes were determined from SPR reflectance imaging.

SPR may also be tailored via nanometer-scale structures,[9] and the ability to pattern such structures in metallic films presents many opportunities. Ebbesen et al.[10] reported enhanced transmission of light through arrays of subwavelength holes in optically thick metallic films, at normal incidence. The enhanced transmission is attributed to initial scattering of the incident light into SPs that penetrate the nanoholes and are again scattered on the other side of the film.[9] The extent of SP generation depends on the combination of incident light wavelength, hole geometry/periodic-

* To whom correspondence should be addressed. E-mail: dsinton@me.uvic.ca. Phone: 250-721-8623. Fax: 250-721-6051. E-mail: rgordon@uvic.ca. Phone: 250-472-5179. Fax: 250-721-6052. E-mail: agbrolo@uvic.ca. Phone: 250-721-7167. Fax: 250-721-7147.

† Department of Mechanical Engineering.

‡ Department of Electrical and Computer Engineering.

§ Department of Chemistry.

(1) Nice, E. C.; Catimel, B. *BioEssays* **1999**, *21*, 339−352.
(2) Homola, J. *Anal. Bioanal. Chem.* **2003**, *377*, 528−539.
(3) Homola, J.; Yee, S. S.; Gauglitz, G. *Sens. Actuators, B* **1999**, *54*, 3−15.
(4) Cooper, M. A. *Anal. Bioanal. Chem.* **2003**, *377*, 834−842.
(5) Mullett, W. M.; Lai, E. P. C.; Yeung, J. M. *Methods* **2000**, *22*, 77−91.
(6) Jung, L. S.; Campbell, C. T.; Chinowsky, T. M.; Mar, M. N.; Yee, S. S. *Langmuir* **1998**, *14*, 5636−5648.
(7) Kim, I. T.; Kihm, K. D. *Exp. Fluids* **2006**, *41*, 905−916.
(8) Iwasaki, Y.; Tobita, T.; Kurihara, K.; Horiuchi, T.; Suzuki, K.; Niwa, O. *Meas. Sci. Technol.* **2006**, *17*, 3184−3188.
(9) Barnes, W. L.; Dereux, A.; Ebbesen, T. W. *Nature* **2003**, *424*, 824−830.
(10) Ebbesen, T. W.; Lezec, H. J.; Ghaemi, H. F.; Thio, T.; Wolff, P. A. *Nature* **1998**, *391*, 667−669.



10.1021/ac070001a CCC: $37.00 
Published on Web 04/21/2007

ity and material/medium dielectric constants. For wavelengths that satisfy SPR conditions for a given system, incident light transmission can be higher than that expected based on area of the nanoholes. This finding is in stark contrast to classical theory[11] that would predict a much lower transmission through subwavelength apertures. The result is a wavelength- and medium-sensitive subwavelength focusing mechanism that has potential applications in several areas including optical filters,[12] imaging,[13] nanolithography,[14,15] photonic circuits,[16] and others. The central role of SPs in the enhanced transmission has motivated the application of nanohole arrays to surface-based chemical and biological detection. The unique optical properties of nanohole arrays and their application in this area have recently been investigated by our group,[17−24] and others.[25−31]

In the context of on-chip chemical and biological analysis, nanohole arrays have several unique advantages: (1) in contrast to reflective mode SPR, transmission mode operation at normal incidence simplifies alignment, facilitates the use of high numerical aperture optics,[29] and permits eventual device-level miniaturization and integration of supporting optics; (2) the footprint of a nanohole array is small relative to that typically required in reflective mode SPR,[28] enabling miniaturization and integration into microfluidic architectures, and higher spatial resolution; (3) in contrast to other local surface plasmon strategies based on colloidal nanoparticles,[32] or roughened surfaces, nanohole arrays can be fabricated with high reproducibility; (4) the high sensitivity of the optical response to hole shape,[22,33] periodicity, and lattice versus basis orientation[23] provides a large variety of handles with which to tailor array/sensor response; and (5) the unique geometry differentiating each array element is fixed within the structure and is generally more robust than an adsorbed probe. A perceived disadvantage of grating-based SPR systems is reduced sensitivity compared to the Kretschmann configuration; however, significantly improved sensitivities have recently been achieved for arrays of nanoholes.[28,29] Motivated by the above advantages, we have demonstrated the application of nanohole arrays to detect the binding of organic and biological molecules.[19] In that case, a shift of the SPR peak in the transmission spectrum from normal incident white light was detected following the adsorption of a mercaptoundecanoic acid monolayer and also subsequent to absorption of a bovine serum albumin. The sensitivity was found to be 400 nm per refractive index.[19] Lui et al. presented an affinity biosensor platform utilizing enhanced fluorescence transduction and demonstrated that enhanced fluorescence output may be obtained in both periodic and randomly distributed nanocavities.[26] The polarization properties of nanohole arrays have been exploited to achieve significantly higher sensitivity at near-normal incidence.[29] In work to date, the confinement offered by a simple microfluidic channel has already proved useful in the delivery of solutions to an array.[26,29] The focus, however, has been on the characteristic optical phenomena from an isolated nanohole array and the unique sensing opportunities provided. The incorporation of arrays of nanohole arrays within a microfluidic framework for spatial and temporal detection on-chip is a natural progression of this technology.

Here we demonstrate nanohole arrays as discrete, 20 $\mu$m × 20 $\mu$m, sensing elements capable of both chemical sensing and biomolecule adsorption monitoring for spatial/temporal measurements in a microfluidic chip platform. The integrated device is manufactured using established soft lithographic microfabrication and focused ion beam nanofabrication. Sensitivity and proof-of-concept tests are performed using a microscope and fiber-optic spectroscopy. The sensor is applied to detect changes in refractive index in sucrose solutions of varying concentration, to measure cross-stream concentration gradients, and to monitor surface binding events.

## EXPERIMENTAL SETUP

**Nanohole Array Fabrication.** Figure 1 shows the arrangement of nanoholes and integration into the microfluidic chip. The nanohole arrays were fabricated by focused ion beam milling on a 100-nm optically thick commercially coated gold film on a 25.4 mm × 25.4 mm glass substrate. The arrays were fabricated and imaged using a FEI 235 dual-beam gallium ion beam and field emission scanning electron microscope. The ion beam was set to 30 keV with a milling rate of 1.6 nm/$\mu$s, and the beam current was 300 nA. The nanoholes were ∼150 nm in diameter and were made to form two rows of six arrays each. One row contained arrays of periodicity (center-to-center spacing between holes) 350, 450, 550, 650, 750, and 850 nm, and the second row contained 6 arrays of 650 nm periodicity. The individual nanohole arrays were ∼20 $\mu$m × 20 $\mu$m each, and the footprint of the entire set of arrays was less than 1 mm × 100 $\mu$m. The sensor array was positioned off center such that the fluidic connections could be maximally separated from the microscope objective during operation.

**Microfluidic Chip Fabrication and Integration.** The microfluidic channel structures were produced using established soft


(11) Bethe, H. A. *Phys. Rev.* **1944**, *66*, 163−182.
(12) DiMaio, J. R.; Ballato, J. *Opt. Express* **2006**, *14*, 2380−2384.
(13) Smolyaninov, I. I.; Elliott, J.; Zayats, A. V.; Davis, C. C. *Phys. Rev. Lett.* **2005**, *94*, 057401.
(14) Srituravanich, W.; Durant, S.; Lee, H.; Sun, C.; Zhang, X. *J. Vac. Sci. Technol. B* **2005**, *23*, 2636−2639.
(15) Srituravanich, W.; Fang, N.; Sun, C.; Luo, Q.; Zhang, X. *Nano Lett.* **2004**, *4*, 1085−1088.
(16) Yin, L. L.; Vlasko-Vlasov, V. K.; Pearson, J.; Hiller, J. M.; Hua, J.; Welp, U.; Brown, D. E.; Kimball, C. W. *Nano Lett.* **2005**, *5*, 1399−1402.
(17) Gordon, R.; Kumar, L. K. S.; Brolo, A. G. *IEEE Trans. Nanotechnol.* **2006**, *5*, 291−294.
(18) Brolo, A. G.; Arctander, E.; Gordon, R.; Leathem, B.; Kavanagh, K. L. *Nano Lett.* **2004**, *4*, 2015−2018.
(19) Brolo, A. G.; Gordon, R.; Leathem, B.; Kavanagh, K. L. *Langmuir* **2004**, *20*, 4813−4815.
(20) Brolo, A. G.; Kwok, S. C.; Moffitt, M. G.; Gordon, R.; Riordon, J.; Kavanagh, K. L. *J. Am. Chem. Soc.* **2005**, *127*, 14936−14941.
(21) Brolo, A. G.; Kwok, S. C.; Cooper, M. D.; Moffitt, M. G.; Wang, C. W.; Gordon, R.; Riordon, J.; Kavanagh, K. L. *J. Phys. Chem. B* **2006**, *110*, 8307−8313.
(22) Gordon, R.; Brolo, A. G.; McKinnon, A.; Rajora, A.; Leathem, B.; Kavanagh, K. L. *Phys. Rev. Lett.* **2004**, *92*, 037401.
(23) Gordon, R.; Hughes, M.; Leathem, B.; Kavanagh, K. L.; Brolo, A. G. *Nano Lett.* **2005**, *5*, 1243−1246.
(24) Gordon, R.; Brolo, A. G. *Opt. Express* **2005**, *13*, 1933−1938.
(25) Liu, Y.; Blair, S. *Opt. Lett.* **2003**, *28*, 507−509.
(26) Liu, Y.; Bishop, J.; Willians, L.; Blair, S.; Herron, J. *Nanotechnology* **2004**, *15*, 1368−1374.
(27) Willians, S. M.; Stafford, A. D.; Rodriguez, K. R.; Rogers, T. M.; Coe, J. V. *J. Phys. Chem. B* **2003**, *107*, 11871−11879.
(28) Stark, P. R. H.; Halleck, A. E.; Larson, D. N. *Methods* **2005**, *37*, 37−47.
(29) Tetz, K. A.; Pang, L.; Fainman, Y. *Opt. Lett.* **2006**, *31*, 1528−1530.
(30) Dintinger, J.; Klein, S.; Ebbesen, T. W. *Adv. Mater.* **2006**, *18*, 1267−1270.
(31) Rindzevicius, T.; Alaverdyan, Y.; Dahlin, A.; Hook, F.; Sutherland, D. S.; Kall, M. *Nano Lett.* **2005**, *5*, 2335−2339.
(32) Sun, Y. G.; Xia, Y. N. *Analyst* **2003**, *128*, 686−691.
(33) Koerkamp, K. J. K.; Enoch, S.; Segerink, F. B.; Hulst, N. F. v.; Kuipers, L. *Phys. Rev. Lett.* **2004**, *92*, 183901.

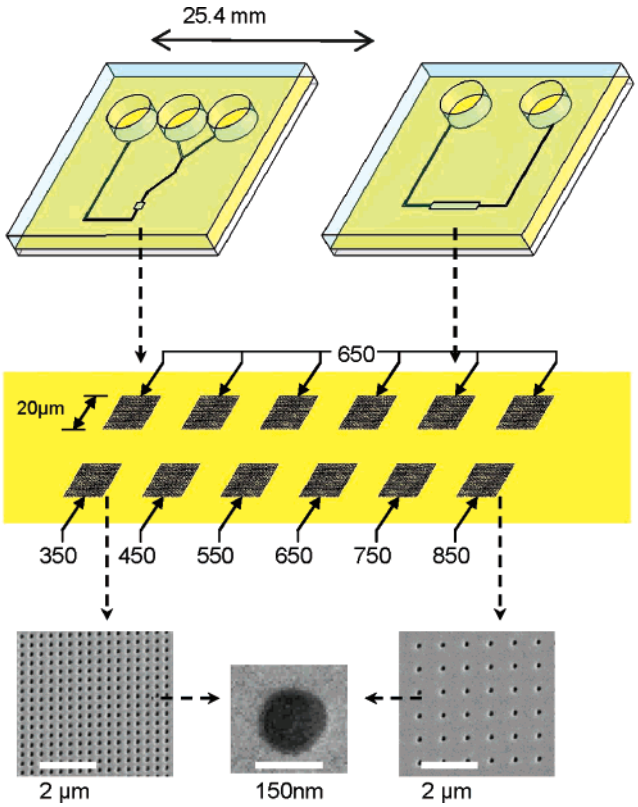


**Figure 1.** Schematic and images illustrating the architecture of the microfluidic chip with embedded nanohole arrays at relevant centimeter-, micrometer-, and nanometer-length scales. Shown are two microfluidic configurations, the sensing element pattern with periodicities indicated, and sample SEM images of the nanoholes (scale bar size indicated.)

lithography techniques.[34,35] Briefly, photomasks of each channel structure were created and printed on transparencies using high-resolution printing. The photoresist SU-8 50 was spin-coated on a silicon wafer ramping to 500 rpm in 5 s, then dwelling for 8 s, then ramping to 2000 rpm in 5 s, and spinning for 25 s, resulting in a uniform thickness of 50 $\mu$m. The coated silicon wafers were prebaked at 65 °C for 6 min and then at 95 °C for 20 min to harden the photoresist. The photomask was positioned over the silicon wafer, and it was exposed under collimated UV light for 45 s. This was followed by a hard bake, first at 65 °C for 1 min and then at 95 °C for 5 min to promote polymerization of the photoresist. The exposed silicon wafer was then immersed in SU-8 developer until all the unexposed photoresist was removed, creating the master templates. The microchannel structures were created by curing 4 mm of PDMS on the masters. This PDMS thickness enabled direct tubing connection via friction fit and ensured channel stiffness under suction. The PDMS was then degassed for 45 min in vacuum and cured at 95 °C for 2 h. The PDMS channel structure was cut from the master, holes for tubing connections were punched, and the PDMS surface was exposed to oxygen plasma for 20 s. The oxygen plasma treatment rendered the PDMS surface hydrophilic and facilitated filling of the device. Irreversible bonding via plasma treatment, as with PDMS−PDMS or PDMS−glass interfaces,[35] is not possible with PDMS−gold. Instead, a conformal bond, reversible seal was employed and the seal was mechanically ensured via an acrylic top plate and clamping mechanism. The top plate was machined to allow tubing connections to the PDMS layer and direct optical access to the area of the chip containing the sensor array. This layered configuration enabled chip disassembly, cleaning of the arrays,[19] and switching of the microfluidic layers as required. In this work, the same multiarray gold-on-glass substrate was employed with over 10 microfluidic structures. The size of the chip assembly was ~7.5 × 25.4 × 25.4 mm$^3$.

**Chemicals.** Solutions of known and controllable refractive indices were required to establish the sensitivity of the nanohole array sensors and to demonstrate local chemical detection within the microfluidic framework. Aqueous sucrose solutions of refractive index varying from 1.332 (pure water) to 1.359 (concentrated sucrose solution) were employed. The refractive index of each solution was determined with a refractometer. For measurements across on-chip-generated concentration gradients, a sucrose solution with a refractive index of 1.359 was used in conjunction with pure water. The sucrose concentration profile across the sensor array was varied with flow rate. Napthol blue black, mixed at 1% by weight in distilled water, was employed to demonstrate the generation of a cross-stream concentration gradient across the sensor array. Chemicals employed in the microfabrication are discussed in the microfabrication section above, and details of the chemicals employed in the on-chip assembly of the cysteamine−biotin−streptavidin system are provided with the results. Volume flow rate of solutions to/from inlets/outlets was ensured via a syringe pump. When possible, the chip was operated in vacuum mode (applying a suction pressure to the outlet) rather than positive pressure at an inlet. Operation in vacuum mode promotes sealing of the channel structure, which is an advantage when a reversible seal is employed.

**Optical Measurements.** Figure 2 shows a schematic of the setup for the optical measurements. A broadband white light from a halogen light source was provided to the nanohole arrays at normal incidence through a 50× long working distance microscope objective (Leica Microsystems, Wetzlar, Germany). This objective ensured that only one array (20 $\mu$m × 20 $\mu$m) received the incident light, and the 8.1-mm working distance provided ample clearance for the assembled chip. Transmission spectra through the nanohole arrays were obtained with a fiber-optic cable connected to a spectrometer. The transmitted light intensity was digitally recorded, in counts, versus wavelength in the range $\lambda$ = 370−1050 nm.

## RESULTS AND DISCUSSION

Figure 1 shows the architecture of the chip at relevant centimeter-, micrometer-, and nanometer-length scales. Two configurations of the microfluidic layer, shown at the top of Figure 1, were developed to deliver solutions to the nanohole array sensors. The most basic configuration is a single-inlet, single-outlet channel with an expanded section to facilitate alignment with the sensor array (top right in Figure 1). This arrangement ensures all arrays experience similar conditions and was used to compare differences between arrays based on periodicity and to acquire redundant measurements on similar arrays sampling the same solution. The second microfluidic layer configuration (shown top

(34) Duffy, D. C.; McDonald, J. C.; Schueller, O. J. A.; Whitesides, G. M. *Anal. Chem.* **1998**, *70*, 4974−4984.
(35) McDonald, J. C.; Duffy, D. C.; Anderson, J. R.; Chiu, D. T.; Wu, H. K.; Schueller, O. J. A.; Whitesides, G. M. *Electrophoresis* **2000**, *21*, 27−40.

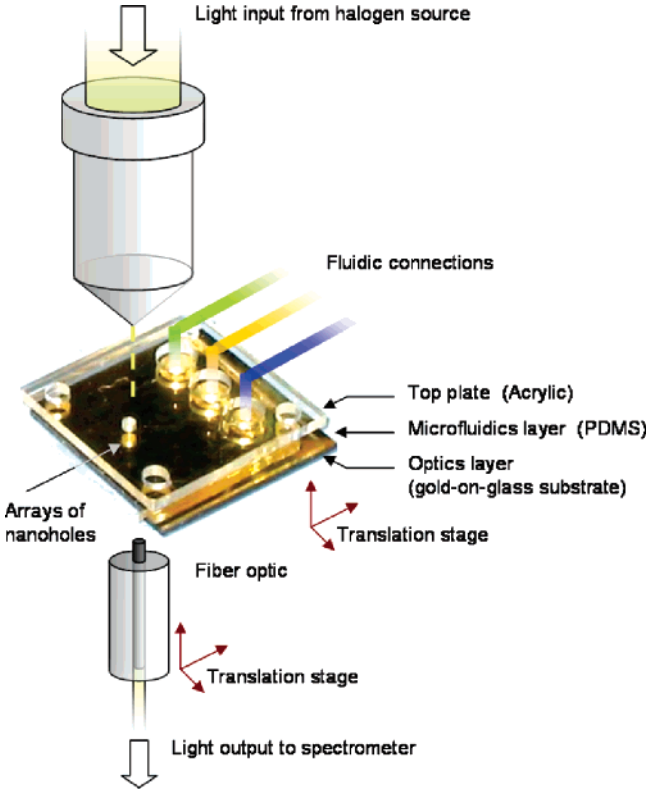


**Figure 2.** Schematic of the transmission mode optical configuration and the fluidic connections employed with the assembled device (image).

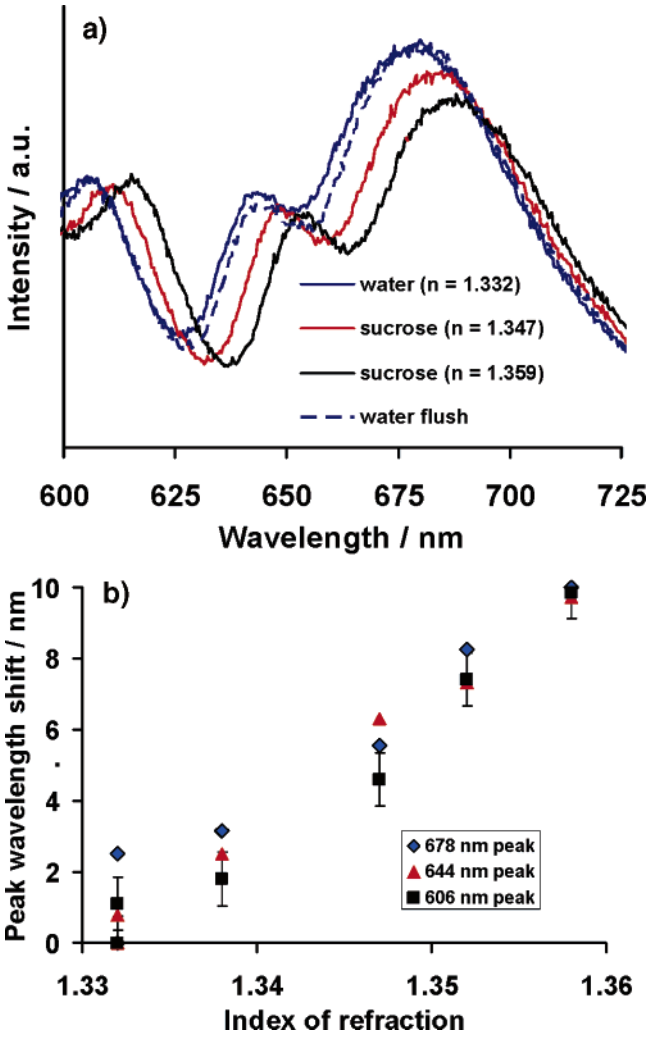


**Figure 3.** Results of sensitivity test employing sucrose solutions of known refractive indices. Transmission spectra were obtained through the 450-nm periodicity array for the cases of pure water, sucrose solutions with increasing refractive index, and again for water. (a) Sample transmission spectra plotted together. (b) The relative red-shift in peak wavelength for three SPR peaks (at wavelengths 606, 644, and 674 nm) exhibited by the array as a function of refractive index. The two sets of data for the pure water case ($n$ = 1.332) correspond to the first and last measurements. Estimated error for all measurements is indicated for the 606-nm wavelength case.

left in Figure 1) has two inlets, one outlet, and an expanded section to deliver flow rate-controlled cross-stream concentration variations during colaminar flow. The sensor array was composed of two rows of nanohole arrays, offset from the center of the substrate to facilitate tubing (world-to-chip interface) without interfering with the collinear optical access. One row contained 650-nm periodicity arrays, and the second row contained arrays differing in periodicity from 350 to 850 nm. Periodicities in this range were selected, as they result in wavelength-specific, SP-enhanced transmission of light in the visible spectrum, to which the spectrometer is sensitive. Portions of the 350- and 850-nm periodicity arrays and a representative nanohole, imaged through scanning electron microscopy, are shown in the lower portion of Figure 1.

As a preliminary test, transmission spectra obtained directly from the nanohole array in air, without a PDMS channel, were compared with those obtained from the assembled chip without any solution. Wavelength- and periodicity-specific enhanced transmission of incident light was evident in both cases, and the measured wavelengths of peak transmission were similar to the limit of detector resolution. All subsequent measurements were obtained with the assembled chip under dynamic solution flow. Five sucrose solutions with known refractive indices varying from 1.332 (pure water) to 1.359 were employed to quantify the sensitivity of the device. A transmission spectrum from each array was obtained on chip for the pure water case, and all sucrose solutions. Following the sucrose solutions, pure water was reintroduced into the chip and a transmission spectrum was obtained.

Figure 3a shows spectra collected for the pure water case, two sugar solutions spanning the range, and the final pure water rinse for the 450-nm periodicity array. The general form of the transmission spectrum is a product of several factors. The periodicity determines the wavelength(s), upon which surface plasmon resonances are excited leading to enhanced transmission.[9,10] Several resonance conditions can be satisfied for a given nanohole array periodicity, and multiple peaks are generally observed from a broadband input. Other influencing factors include the power spectrum of the light input and the sensitivity of the detector as a function of wavelength. From the perspective of chemical and biological sensing, the transmission spectrum should exhibit SP-induced definable features (high gradients), and the spectral shift in those features should be a predictable function of near-surface refractive index attributable to concentration or surface binding. As shown in Figure 3a, the spectrum is red-shifted in response to solutions with increased refractive index. The red-shift shown for the 450-nm periodicity array in Figure 3a was

representative of the response of the other arrays in agreement with established theory of light transmission through nanoholes.[10,36] In the case of the 850- and 750-nm periodicity arrays, however, the intensity of the main resonance peak occurred at wavelengths beyond the efficient range of the detector. Therefore, the spectral shifts from the 750- and 850-nm periodicity arrays, although similar to those observed in the 350−650-nm periodicity arrays, could not be quantified with the same accuracy. The redshift in the three peak wavelengths shown in Figure 3a were recorded as a function of solution refractive index with the results plotted in Figure 3b. Error bars representative for all measurements are indicated on the 606-nm wavelength peak case, and the two sets of data for the pure water case correspond to the first and last measurements. The plot indicates that increasing the index of refraction over the total range, 0−2%, resulted in a significant, linear increase in relative peak wavelength from 0 to 10 nm. Also, the first and last pure water measurements collapse well near $n = 1.332$ as expected. The demonstrated sensitivity is 333 nm/refractive index unit (RIU) in very good agreement with previous measurements with similar arrays and experimental setup.[19]

Figure 4a shows a microscope image of a cross-stream concentration gradient in the Y-channel configuration. The set of six, 650-nm periodicity arrays were employed to spatially resolve a cross-stream concentration gradient in a microfluidic flow. Several applications of microfluidics to concentration gradient generation have been motivated by the importance of concentration gradients to biological processes[37] and interest in monitoring molecular interactions.[38,39] Microfluidic gradient generation was facilitated here by colaminar microfluidic streaming from the Y-channel intersection geometry shown in Figure 1. Due to the laminar nature of the flow, mixing was limited to diffusion alone, and the width of the mixing region of the two adjacent liquid streams could be controlled by varying the flow rate. In the case of ideal, pluglike, electroosmotic flow, the mixing process is one-dimensional. Cross-stream velocity gradients in pressure-driven flows, however, result in more rapid mixing near the microchannel walls than at the midplane.[40] Nanohole array sensors sample exclusively in the near-wall region where the mixing width can be expected to scale as $(Dh_C y/U)^{1/3}$, where $D$ is the diffusion coefficient, $U$ is the average flow speed in the channel, $h_C$ is the channel height, and $y$ is the distance traveled along the channel.[40] Characteristic near-wall mixing widths were estimated based on the Y-channel configuration shown in Figure 1, with a diffusion coefficient of $5 \times 10^{-10}$ m$^2$/s, channel height of 50 $\mu$m, channel width of 200 $\mu$m, and mixing distance of 7 mm (between the intersection and the expanded region containing the nanohole arrays). Flow rates of 0.001 and 0.050 mL/min resulted in mixing width length scales corresponding to 24 and 7% of the channel width, respectively. A colored dye solution was employed to demonstrate the gradient generation across the expanded region at 0.001 mL/min. The dye was introduced at one inlet while the other inlet provided pure water. The generated concentration gradient is effectively spread across the expanded region containing the arrays and reformed at the outlet. Due to the increased channel width in this region, negligible cross-stream mixing is expected despite the relatively long residence time. Similar geometries have been employed to increase axial diffusion at the expense of cross-stream mixing.[41]

Marker-free concentration detection was achieved here using the six 650-nm periodicity arrays labeled in the image in Figure 4a. The dye solution was replaced with a sucrose solution, and the resonance peak wavelengths were recorded at each cross-stream 650-nm periodicity array under different flow rates. The distribution of the sensor arrays shown in Figure 4a indicates that array 6 would be expected to sample the pure water stream, and given identical flow rates of each solution, the mean concentration would be expected along the centerline between arrays 2 and 3.

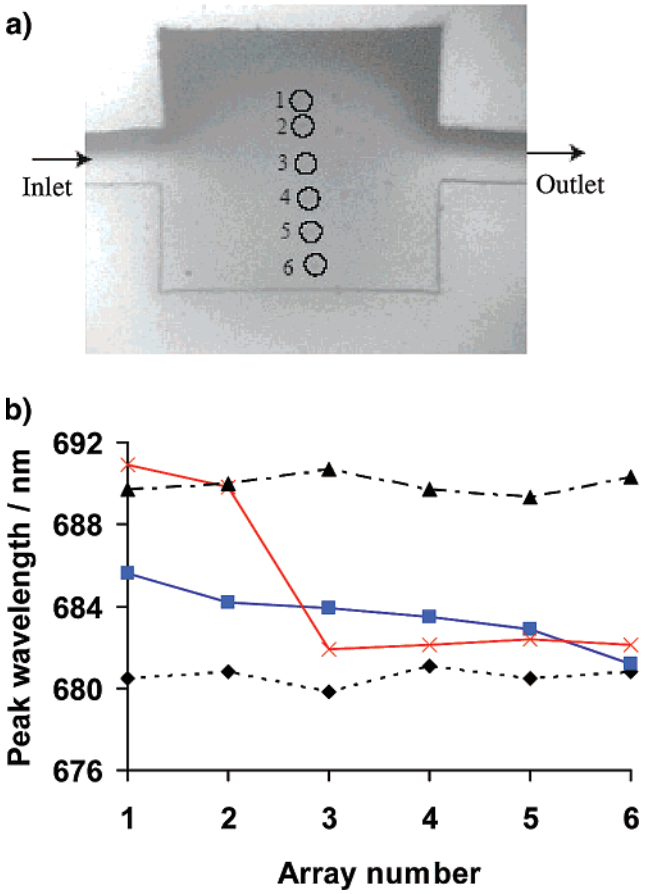


**Figure 4.** Application of spatially separated (similar periodicity) nanohole arrays to resolve a cross-stream concentration gradient in a microfluidic flow. (a) A 5× magnification image of colored dye (instead of sucrose solution) to demonstrate gradient generation across the arrays at a flow rate of 0.001 mL/min. The array periodicity is 650 nm. (b) A plot of resonance wavelength for each of the six arrays for the cases of uniform water solution (diamonds and dotted line), uniform sucrose solution (triangles and dot-dash line), and gradient generation at 0.001 (blue squares and line) and 0.05 mL/min (red line and crosses). Array numbers correspond to those labeled in (a).

(36) Krishnan, A.; Thio, T.; Kima, T. J.; Lezec, H. J.; Ebbesen, T. W.; Wolff, P. A.; Pendry, J.; Martin-Moreno, L.; Garcia-Vidal, F. J. *Opt. Commun.* **2001**, *200*, 1−7.
(37) Dertinger, S. K. W.; Chiu, D. T.; Jeon, N. L.; Whitesides, G. M. *Anal. Chem.* **2001**, *73*, 1240−1246.
(38) Hatch, A.; Kamholz, A. E.; Hawkins, K. R.; Munson, M. S.; Schilling, E. A.; Weigl, B. H.; Yager, P. *Nat. Biotechnol.* **2001**, *19*, 461−465.
(39) Kamholz, A. E.; Weigl, B. H.; Finlayson, B. A.; Yager, P. *Anal. Chem.* **1999**, *71*, 5340−5347.
(40) Ismagilov, R. F.; Stroock, A. D.; Kenis, P. J. A.; Whitesides, G.; Stone, H. A. *Appl. Phys. Lett.* **2000**, *76*, 2376−2378.
(41) Coleman, J. T.; McKechnie, J.; Sinton, D. *Lab Chip* **2006**, *6*, 1033−1039.

Figure 4b compares the resonance wavelength recorded at each cross-stream array when the channel contained pure water, pure sucrose solution, a gradual gradient (0.001 mL/min), and a sharper gradient (0.05 mL/min). The resulting resonance wavelength profiles reflect expected cross-stream concentration behavior in each case. Specifically, the resonance wavelength was consistent across the channel for the pure water case and showed a uniform ~10-nm red-shift in response to the sucrose solution. At both focusing flow rates, array 6 reported very little deviation in resonance wavelength from the pure water case. The expected shapes of both the sharp (0.05 mL/min) and more gradual (0.001 mL/min) gradient are reflected in progressive red-shifts in arrays 5 through 1. The monotonic increase in red-shift in the case of the gradual gradient is in qualitative agreement with prediction based on flow rate although it is difficult to estimate the width of the mixing zone other than that it is less than the channel width. In the case of the sharper gradient, the near-wall mixing region is found to be confined at the centerline between arrays 2 and 3, indicating a mixing length on the order of 10% of the channel width, in agreement with the scaling analysis above.

In analogy with traditional bioanalytical applications of SPR,[5,42,43] it is expected that on-chip SPR-based sensors will find most utility where the surface-specific nature of SPs can be exploited; in the monitoring of adsorption processes. The surface-specific nature of nanohole array-based sensing was exploited here to monitor surface binding events of biological molecules in a flow-through microfluidic format. The cysteamine−biotin−streptavidin model system was chosen because it is readily available, the biotin−streptavidin bond is generally quite strong, and the biochemistry is well established.[44] A schematic of the final protein binding is shown in Figure 5a, and it is a product of a three-part process. First, a solution of cysteamine with a molar mass of 65 g/mol was prepared (0.002 g of cysteamine in 5 mL of water). The arrays of nanoholes were rinsed with acetone and methanol, placed in an ultrasonic bath in methanol for 3 min, plasma cleaned for 15 min, and immersed in the cysteamine solution for 72 h to assemble a monolayer on the gold surface. The gold chip was removed from the cysteamine solution after the monolayer formation and cleaned with ethanol and with distilled water. The microfluidic device was then assembled, the PDMS channel structure and cover plate were aligned and clamped over the gold-on-glass substrate, and the channels were filled with pH 7 phosphate buffer solution (PBS). The transmission spectrum from each 650-nm periodicity array was obtained. In the second step, a solution of biotin linker (EZ-Link NHS-LC−LC-Biotin) was prepared by dissolving 12 mg of biotin into 2 mL of dimethyl sulfoxide (DMSO). This biotin solution was introduced to the cysteamine monolayer via the microfluidic chip for 45 min at a rate of 0.02 mL/min. The chip was flushed with PBS buffer solution, and the transmission spectrum from each 650-nm periodicity array was obtained.

The third and final step in the protein binding experiment involved the streptavidin protein solution (~1 mg of streptavidin dissolved in 4 mL of PBS buffer). The nanohole arrays were exposed to the streptavidin solution for 15 min at a flow rate of 0.02 mL/min. The transmission spectra were then obtained with the streptavidin−PBS solution in the channel and following a flush with PBS buffer. The SPR peaks from each step in the flow-through assembly process were measured. The wavelength shifts ($\Delta\lambda$) were calculated using the SPR peak of cysteamine as reference and plotted in Figure 5b. The total surface group assembly process corresponded to resonance peak red-shifts of ~3.5−4 nm, indicating an increased surface-average refractive index as expected from protein adsorption.[45] Results were analyzed from each of the six arrays in three separate runs. The error bars in Figure 5b correspond to the standard deviation calculated for a particular run. The scatter in the biotin data was typical in the assembly runs conducted. This may be due to the use of the organic solvent (DMSO), which may remain as trace contamination during the rinsing or introduce some impurities into the system by interacting with the PDMS. A decreased response from arrays close to the lateral wall of the microchannel (for instance, see arrays 5 and 6 in Figure 3) was observed in one of the runs, and this was attributed to partial removal/damage of the cysteamine monolayer during alignment. The shifts measured with streptavidin in solution decreased by 1 nm after flushing with the PBS solution. The change in SPR peak following the final rinse indicates both the formation of adsorbed proteins and the surface-specific nature of the SPR-based sensors. The magnitude of the

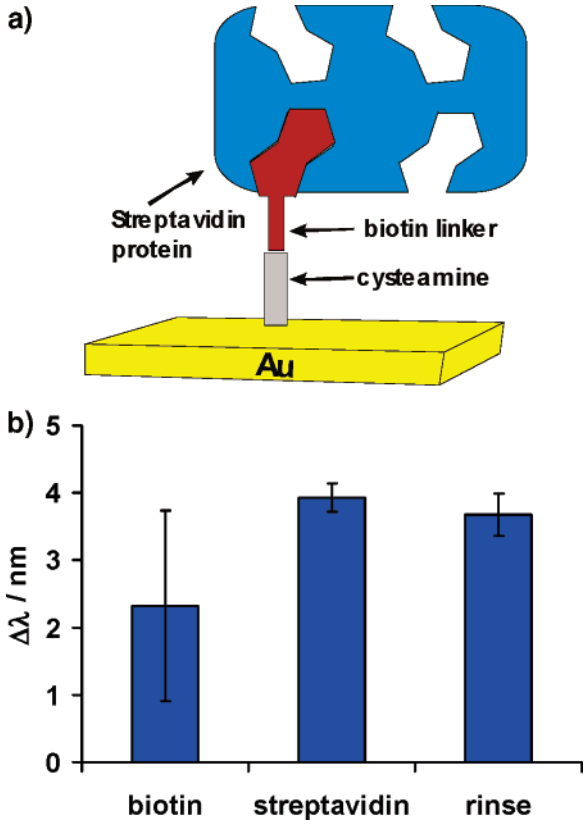


**Figure 5.** Application of on-chip nanohole arrays to detect surface binding in the assembly process of a cysteamine monolayer−biotin linker−streptavidin protein system. (a) Schematic of the streptavidin protein binding strategy. The four biotin binding sites present in streptavidin are indicated. (b) SPR shift measured relative to cysteamine after the addition of biotin, streptavidin, and PBS rinsing.

(42) Frutos, A. G.; Corn, R. M. *Anal. Chem.* **1998**, *70*, 449a−455a.
(43) Hanken, D. G.; Jordan, C. E.; Frey, B. L.; Corn, R. M. *Electroanal. Chem.* **1998**, *20*, 141−225.
(44) Neuert, G.; Kufer, S.; Benoit, M.; Gaub, H. E. *Rev. Sci. Instrum.* **2005**, *76*, 054303.
(45) Jung, L. S.; Nelson, K. E.; Campbell, C. T.; Stayton, P. S.; Yee, S. S.; Perez-Luna, V.; Lopez, G. P. *Sens. Actuators, B: Chem.* **1999**, *54*, 137−144.

shifts reported here are in general agreement with earlier experimental work by our group,[19] but not as high as reported by others.[28,29]

The sensitivity of the nanohole integrated device in resonance units (RU), where 1 RU is 1 pg of biomaterial/mm$^2$ of the sensor surface, was estimated using the methodology described elsewhere.[6] The slope of the refractive index calibration (Figure 3), the wavelength shift due to the protein adsorption (Figure 5), an estimated 200-nm decay length for the SP field,[36,46] and a specific volume of 0.71 cm$^3$/g for the protein[47] were used in the calculation. A sensitivity of ~6500 RU was obtained from our data. Typical sensitivity values from commercial SPR devices are ~70 000 RU. It is important to emphasize that the sensitivity is not a fundamental limitation for the array of nanoholes, and it can match the observed from typical commercial SPR systems. The sensitivity reported here could be easily improved by using a laser source combined to a better detection system.[28] The geometric parameters of the array can also be tailored to increase sensitivity. For instance, the periodicity could be designed to allow the match between the SPR resonance and the laser source,[28] and substrates with optimized hole diameter[29] and shape[48] would lead to sharper resonances and provide polarization-sensitive response. Moreover, the amount of protein in the microchannel during incubation (17.5 $\mu$g) and the sample volume of our microfluidic sensing chamber (0.05 $\mu$L) are comparable to commercial devices (Biacore X, for instance). However, as can be seen in Figure 1, our device supports 12 sensing elements (arrays) within this volume.

The benefits of nanohole arrays for on-chip detection, as demonstrated in this paper, are balanced by some limitations. Due to the inherent surface-specific nature of surface plasmons, the detection volume is limited to the near-surface region. The response to refractive index changes is also not selective. As in a typical SPR instrument, the specificity of the sensor is given by the immobilization of appropriated targets. Also, in contrast to electrochemical-based detection methods, optical access and associated optical infrastructure are required for nanohole-based detection. Sensitivity of nanohole arrays has previously been demonstrated to be similar to commercial SPR systems;[28,29] however, the additional optical processing and infrastructure required present some additional cost as compared to the relatively simple setup employed here. Last, fabrication of the nanohole arrays via focused ion beam milling, as employed here, is relatively expensive. Effective nanohole array fabrication has, however, also been demonstrated using photolithography.[29,49]

The results presented here effectively demonstrate nanohole arrays as SPR-based sensing elements in a microfluidic platform. Discrete nanohole arrays serve as effective on-chip sensing elements and fit well with the existing microarray concept. An alternative architecture would be a continuously perforated metallic film as a substrate for whole-chip monitoring. Integrated with small bandwidth sources, such as laser diodes, and CCD detection, imaged intensity could be interpreted directly in terms of surface properties, in real time. Reports on the utilization of arrays of nanoholes fabricated by photolithographic methods are available in the literature,[29,49] indicating that large-area, cost-effective nanohole substrates can in principle be mass produced for widespread applications.

## SUMMARY AND CONCLUSION

A microfluidic device with an integrated array of nanohole arrays serving as SPR-based chemical and biological sensors was developed and demonstrated. Measurements indicate that arrays of nanoholes can be integrated and used as effective SPR detectors in an on-chip format. The integrated device was successfully applied to detect changes in refractive index with a sensitivity of 333 nm/RIU, which is comparable to previously reported values. A set of six, 650-nm periodicity arrays were employed to spatially resolve a cross-stream concentration gradient in a microfluidic flow. The unique surface sensitivity of nanohole arrays was exploited to detect surface binding in the assembly process of a cysteamine monolayer−biotin linker−streptavidin protein system. In gradient-based measurements, cross-stream concentrations determined at different flow rates agreed well with a dye-based experiment and a scaling analysis. In the protein binding event monitoring experiments, average shifts in resonance wavelength of 3.5−4.0 nm were observed. These shifts are in general agreement with earlier experimental work. The results presented here effectively demonstrate the application of nanohole arrays as surface plasmon-based sensing elements in a microfluidic platform. Nanohole array substrates as a platform for chip-based analysis, add unique surface-sensitive diagnostic capabilities to the existing suite of microfluidic-based analytical tools.

## ACKNOWLEDGMENT

The authors are grateful for the financial support of the Natural Sciences and Engineering Research Council (NSERC) of Canada, through discovery research grants, and a postgraduate scholarship to A.D. This work was also supported by equipment grants from the Canada Foundation for Innovation (CFI). A fellowship from the University of Victoria to A.D. is also gratefully acknowledged.

Received for review January 1, 2007. Accepted March 19, 2007.

AC070001A

(46) Chang, S. H.; Gray, S. K.; Schatz, G. C. *Opt. Express* **2005**, *13*, 3150−3165.
(47) Pahler, A.; Hendrickson, W. A.; Kolks, M. A.; Argarana, C. E.; Cantor, C. R. *J. Biol. Chem.* **1987**, *262*, 13933−13937.
(48) Jung, Y. S.; Sun, Z.; Wuenschell, J.; Kim, H. K.; Kaur, P.; Wang, L.; Waldeck, D. *Appl. Phys. Lett.* **2006**, *88*, 243105.
(49) Henzie, J.; Barton, J. E.; Stender, C. L.; Odom, T. W. *Acc. Chem. Res.* **2006**, *39*, 249−257.